PHYSICAL REVIEW A **76**, 023403 (2007)

HD^+ in a short strong laser pulse: Practical consideration of the observability of carrier-envelope phase effects

V. Roudnev* and B. D. Esry
J.R. Macdonald Laboratory and Department of Physics, Kansas State University, Manhattan, Kansas 66506, USA

(Received 2 March 2007; published 9 August 2007)

We summarize the results of numerical calculations of HD^+ in a 7.1 fs (intensity full width at half maximum) 790 nm laser pulse. The molecule is assumed to be aligned with the linearly polarized laser field and includes two electronic and one nuclear degrees of freedom. We report total dissociation and ionization probabilities from the lowest 10 vibrational states for a range of intensities from 10^{13} to 7×10^{14} W/cm^2. The conditions for the observability of carrier-envelope phase (CEP) effects for a mixed initial state and for intensity averaging over the laser focal volume are discussed in detail.

DOI: 10.1103/PhysRevA.76.023403 PACS number(s): 33.80.Wz, 33.80.Rv, 33.80.−b

I. INTRODUCTION

Diatomic molecules and molecular ions in intense laser fields continue to attract the attention of the atomic and molecular physics community despite several years of study. The nonperturbative nature of the laser field coupled with the interplay of the electronic and nuclear degrees of freedom make for very rich physics. It is, of course, precisely these properties that also make these systems such a challenge to treat theoretically.

The hydrogen molecular ion is of special interest since it is the simplest molecule, consisting of three particles only. Even so, it exhibits many interesting intense laser-induced phenomena including vibrational trapping and bond softening [1–5], high harmonic generation [6], above threshold dissociation [1,2,7], and enhanced ionization [8–11]. Other studies [12] have shown that the relative phase between two laser pulses with different central frequencies could be used to control the dissociation of HD^+. The main finding was that the angular distributions of H and D depended differently on the relative phase of the two laser pulses—where H had a maximum, D had a minimum, and vice versa. Rather complete reviews of the behavior of H_2^+ and its isotopes in intense lasers are also available (see, for example, Refs. [13,14]).

The case of few-cycle laser pulses is especially interesting. Recently, it has become possible to observe [15] and control [16] the carrier-envelope phase (CEP) of a single ultrashort laser pulse, i.e., the relative phase between the laser pulse envelope and the carrier wave. To varying degrees, each of these experiments took advantage of the CEP dependence of the electron motion following ionization.[26]

In contrast, our recent predictions [17,18] of CEP effects in HD^+ do not involve ionization. Rather, we predicted strong CEP effects in the dissociation of the ground vibrational state of HD^+ and H_2^+. While certainly related to the effect measured by Kling *et al.* [19], the effects we described in Refs. [17,18] and will elaborate on further here do not rely on ionization, while the Kling *et al.* CEP measurements on D_2 do. On the other hand, experimental investigation of our system is technically difficult since it would require HD^+ (or H_2^+) in its ground vibrational state. In this paper we have considered the more realistic case of incoherent Franck-Condon distribution [20]. To this end, we have performed detailed calculations of HD^+ dissociation and ionization in short [7.1 fs full width at half maximum (FWHM)] laser pulses for different initial vibrational states. We have found that even when the CEP effect on the total dissociation probability is quite small, the fragment kinetic energy release (KER) is much more sensitive to the CEP. We also present the total ionization and dissociation probability of HD^+ in short laser pulses and discuss the conditions most favorable for a well pronounced CEP effect.

II. THEORY AND NUMERICS

Our calculations are based on the scaled coordinate method that we have described in more detail in Ref. [18]. Here we will give only a brief description of the method together with details important for the current calculations.

A. Three-degree-of-freedom model

The results we present in this paper are based on solving the time-dependent Schrödinger equation (TDSE) (atomic units will be used throughout unless otherwise noted)

$$i\frac{\partial}{\partial t}\Psi=[T+V_0+W(t)]\Psi. \tag{1}$$

In this equation, T is the free Hamiltonian of the system, V_0 stands for the Coulomb interactions, and $W(t)$ describes the interaction with the external laser field. A full solution to this problem requires the propagation of a six-dimensional wave function. Unfortunately, this task is beyond our current capability. We must, therefore, use physical reasoning and intuition to reduce the dimensionality to something manageable that also retains the essential physics of the problem. In fact, our goal is to make minimal reductions necessary.

First, let us arrange the time scales describing the dynamics of the system. The slowest process is molecular rotation. The period corresponding to an elementary rotational excita-

---

*Present address: Department of Physics and Astronomy, University of Kentucky, Lexington, KY.

tion $T_{rot} \approx 700$ fs. The next faster time scale corresponds to vibrations of the molecule, and its characteristic time is of the order of 15 fs. The shorter time scales correspond to the laser pulse duration (7.1 fs FWHM), the carrier period of $\sim$2.6 fs, and the even faster electronic motion. Due to the huge difference between the time scales of the rotational motion and the other dynamics, we use the common assumption that the molecule does not rotate appreciably during the laser pulse, and that any rotations do not substantially influence the dynamics. Further, since we are primarily interested in dissociation, the most likely transition is $1s\sigma \rightarrow 2p\sigma$ for which only the component of the laser field parallel to the molecular axis is important. We thus assume that the nuclei are aligned with the field and not rotating. Under these assumptions, the six-dimensional configuration space is reduced to three-dimensional [26–34,38]: (R,ρ,z), where R is the internuclear distance and (ρ,z) are the cylindrical coordinates of the electron. For our model, then, the kinetic energy T in Eq. (1) reads

$$T = -\frac{1}{2\mu_{pd}}\frac{\partial^2}{\partial R^2} - \frac{1}{2\mu_e}\left(\frac{\partial^2}{\partial \rho^2} + \frac{1}{\rho}\frac{\partial}{\partial \rho} + \frac{\partial^2}{\partial z^2}\right), \tag{2}$$

and the Coulomb potential is

$$V_0 = -\frac{1}{\sqrt{[z + z_p(R)]^2 + \rho^2}} - \frac{1}{\sqrt{[z - z_d(R)]^2 + \rho^2}} + \frac{1}{R}. \tag{3}$$

Here $z_p(R) = \frac{m_d}{m_p + m_d}R$ and $z_d(R) = \frac{m_p}{m_p + m_d}R$ are the positions of the proton and deuteron, respectively, m_p and m_d are their masses, and μ_{pd} and μ_e are the reduced masses

$$\frac{1}{\mu_{pd}} = \frac{1}{m_p} + \frac{1}{m_d} \quad \text{and} \quad \frac{1}{\mu_e} = 1 + \frac{1}{m_p + m_d}. \tag{4}$$

The interaction with the laser field is written in the dipole approximation (in the length gauge) as

$$W(t) = -E(t)\left[\frac{m_p - m_d}{m_p + m_d}R + \frac{m_p + m_d + 2}{m_p + m_d + 1}z\right]. \tag{5}$$

Here $E(t)$ stands for the electric component of the laser field. The time dependence of the electric field is represented as

$$E(t) = E_0 e^{-\left(\frac{t}{\tau}\right)^2}\cos(\omega t + \phi), \tag{6}$$

where E_0 is the peak field [39], $\sqrt{2\ln 2}\tau$ is the intensity FWHM pulse duration, ω is the laser frequency, and ϕ is the carrier-envelope phase (CEP) of the pulse. We note that the dc component of the pulse is practically zero ($<10^{-8}$) for all ϕ so long as the pulse duration exceeds roughly one laser period. It is the sensitivity of the dissociation parameters to the CEP ϕ that will be the center of discussion in this paper.

We assume that the initial state of the HD$^+$ ion is a result of fast ionization of the HD molecule [20]. This creation mechanism implies an initial state with a Franck-Condon distribution of the vibrational levels. We also assume that the time between the HD ionization and the resulting HD$^+$ entering the laser focus is very long compared to the vibrational period and that the distribution of these travel times is also broad on the scale of vibrational periods. The different initial vibrational states in the Franck-Condon distribution thus sum incoherently. In order to model this situation, we perform calculations for the lowest 10 vibrational states and sum the corresponding final observables with Franck-Condon weights.

B. Scaled coordinates

One common problem with time-dependent approaches is that they are necessarily limited to a finite integration volume: when part of the physical system reaches the boundary, artifacts due to reflections appear. This problem is often solved via absorbing boundary conditions by introducing an imaginary potential or a masking function. Such boundary conditions, however, lead to lost information. Numerical solutions are further complicated by a phase that accumulates rapidly with time and distance, making the wave function oscillate rapidly. These oscillations make numerical approximation of the wave function difficult, especially when long propagation times are required.

A coordinate scaling technique that addresses both of these problems was originally proposed in a different context in Ref. [35]. A more general point of view on the numerical benefits of this scaling transformation was discussed in Ref. [36,37]. In our preceding paper [18] we discussed in detail the application of the technique to dissociation of HD$^+$. Here, we give just a brief reminder of the method.

The method of scaled coordinates combines coordinate and wave function transformations that localize continuum wave packets in space and essentially eliminates growing spatial oscillations. By analytically eliminating these purely kinematic effects, the wave function can be more easily propagated to larger times. The ability to propagate the wave function longer is essential for calculating the final velocity distributions of these three charged particles: the propagation must be long enough that the final state fragments no longer interact significantly with each other. Another useful feature of the scaled coordinate method is that it affords a straightforward way to extract the velocity distribution from the final state density function—the wave function itself is not required. Further, knowledge of the density function in the whole configuration space is not necessary, as all coordinates corresponding to the internal degrees of freedom of the final state fragments can be integrated out. Taken together, these features make the scaled coordinate approach extremely useful for treating systems in several dimensions.

In this work we scale the internuclear distance R only, using an absorbing optical potential for the electronic coordinates. This choice minimizes the computational effort required to reproduce the atomic wave functions in the final state. Explicitly, as we have described in Ref. [18], we use the following transformations,

$$R = S(t)\xi, \tag{7}$$

for the internuclear distance, plus a wave function transformation

$$\Psi^S(\xi,t) = \sqrt{S}e^{-i(m/2)S\dot{S}\xi^2}\Psi(S\xi,t). \tag{8}$$

The scaling function is chosen as

$$S(t) = \begin{cases} 1, & t < t_0, \\ [1 + v_R^4(t-t_0)^4]^{1/4}, & t \geq t_0. \end{cases} \tag{9}$$

where v_R and t_0 are the scaling parameters that should be chosen to keep the dissociating wave function with the ξ grid during the whole propagation time. After these transformations the operator T reads

$$T = -\frac{1}{2\mu_{pd}S^2}\frac{\partial^2}{\partial\xi^2} + \frac{1}{2}\mu_{pd}S\ddot{S}\xi^2 - \frac{1}{2\mu_e}\left(\frac{\partial^2}{\partial\rho^2} + \frac{1}{\rho}\frac{\partial}{\partial\rho} + \frac{\partial^2}{\partial z^2}\right)$$
$$\equiv T_\xi + T_\rho + T_z.$$

In this approach the potential V_0 in Eq. (3) also becomes time dependent, while additional time dependence is introduced in Eq. (5).

Besides the numerical advantages of the scaling transformation, it also allows one to obtain the kinetic energy distributions of the dissociated fragments directly from the final-state density function, without resorting to a Fourier transform of the final-state wave function. For instance, if we know the scaled final-state density function $\rho(\xi,t)$, the corresponding KER distribution reads

$$\rho(E) = \lim_{t\to\infty}\frac{1}{v_R\sqrt{2\mu_{pd}E}}\rho\left(\frac{1}{v_R}\sqrt{\frac{2E}{\mu_{pd}}},t\right).$$

A more detailed discussion of the properties and application of the scaling transformation to molecular dissociation calculations can be found in our previous paper [18].

C. Final-state channels

As mentioned above, we start from an oriented molecule with the deuteron "down" and the proton "up." Now we have to classify the final states of the system.

First of all, we have to distinguish the states with one, two, and three free particles in the final state. In the first case, after the laser pulse we find the molecule in a bound state, and we shall call this channel "survival." The second case, where the two fragments are a neutral atom and a charged nucleus, we shall call "dissociation." Finally, if the system breaks up into three charged particles, we shall call this channel "ionization." In our calculation the ionized part of the wave function is absorbed at the boundaries, so that only the dissociation and survival channels are kept during the whole period of calculation. We thus estimate the ionization probability by the difference between the initial and final probabilities $P_I = 1 - \int|\Psi_{\text{final}}|^2 dR dz d\rho$. Since we consider heteronuclear molecular ion, two different dissociation channels can be distinguished: H+d and D+p. Dissociation into these channels can be identified by the regions in configuration space where the corresponding wave packets propagate, as shown in Fig. 1. In the region $\Omega_{\text{H+d}}$ the electron stays in the vicinity of the proton forming hydrogen, whereas in $\Omega_{\text{D+p}}$ it stays close to the deuteron forming deuterium.

In order to separate the dissociation and survival channels, we use the simplest projection operators. For instance, we define

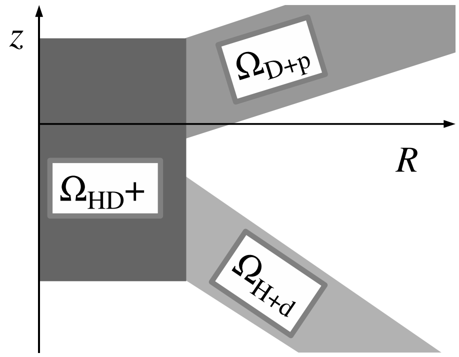

FIG. 1. Configuration space regions associated with different final state channels.

$$\Psi_{\text{H+d}}(R,z,\rho) \equiv \chi_{\Omega_{\text{H+d}}}(R,z,\rho)\Psi(R,z,\rho),$$

where $\chi_{\Omega_{\text{H+d}}}(R,z,\rho)$ is the characteristic function of the region $\Omega_{\text{H+d}}$ defined such that $\chi_{\Omega_{\text{H+d}}}(R,z,\rho)=1$ when the coordinates $(R,z,\rho) \in \Omega_{\text{H+d}}$, and $\chi_{\Omega_{\text{H+d}}}(R,z,\rho)=0$ otherwise. We define the channel functions $\Psi_{\text{D+p}}(R,z,\rho)$ and $\Psi_{\text{HD}^+}(R,z,\rho)$ similarly.

Throughout this paper we shall thus employ the following analysis of the final state: total channel probabilities

$$P_{\text{H+d}} = \int |\Psi^S_{\text{H+d}}(\xi,z,\rho)|^2 d\xi dz d\rho,$$

$$P_{\text{D+p}} = \int |\Psi^S_{\text{D+p}}(\xi,z,\rho)|^2 d\xi dz d\rho, \tag{10}$$

$$P_{\text{HD}^+} = \int |\Psi^S_{\text{HD}^+}(\xi,z,\rho)|^2 d\xi dz d\rho,$$

and fragment kinetic energy release (KER) distributions

$$p_{\text{H+d}}(E) = \frac{1}{v_R\sqrt{2\mu_{pd}E}}d_{\text{H+d}}\left(\frac{1}{v_R}\sqrt{\frac{2E}{\mu_{pd}}}\right),$$
$$p_{\text{D+p}}(E) = \frac{1}{v_R\sqrt{2\mu_{pd}E}}d_{\text{D+p}}\left(\frac{1}{v_R}\sqrt{\frac{2E}{\mu_{pd}}}\right), \tag{11}$$

where

$$d_{\text{H+d}}(\xi) = \int |\Psi^S_{\text{H+d}}(\xi,z,\rho)|^2 dz d\rho,$$

$$d_{\text{D+p}}(\xi) = \int |\Psi^S_{\text{D+p}}(\xi,z,\rho)|^2 dz d\rho.$$

D. Calculations

1. Time propagation

Solutions of the TDSE can be found using the short-time propagator

$$\psi(t+\delta) \approx e^{-i[T+V(t+\delta/2)]\delta}\psi(t) \tag{12}$$

which we evaluate using operator splitting,

$$e^{-i(A+B)\delta} = e^{-iA\delta/2}e^{-iB\delta}e^{-iA\delta/2} + O(\delta^3).$$

The exponentials can be evaluated in a number of ways, but we choose a Crank-Nicholson-like method [41]:

$$U_A(\delta) = \left(1 + iA\frac{\delta}{2}\right)^{-1}\left(1 - iA\frac{\delta}{2}\right) = e^{-iA\delta} + O(\delta^3). \tag{13}$$

With sufficiently small time steps δ, the evolution operator can be represented to a required precision.

To construct the full three-dimensional evolution operator, we split the kinetic from the potential energy operators, taking into account the fact that the kinetic energy operators T_ξ, T_ρ, and T_z commute. An approximate evolution operator is thus

$$U(t+\delta,t) = U_V\left(\frac{\delta}{2};t\right)U_{T_\xi}(\delta)U_{T_\rho}(\delta)U_{T_z}(\delta)U_V\left(\frac{\delta}{2};t\right). \tag{14}$$

We evaluate the kinetic energies using a three-point finite difference scheme capable of treating non-Cartesian coordinates on a nonuniform grid [40]. The potential operator V includes all the potential energy of the system plus the absorbing potential V_A, so that

$$V = V_0 + W\left(t + \frac{\delta}{2}\right) + V_A.$$

Equation (14) can be used for calculations, but explicitly exploiting the different physical time-scales of the system speeds the calculations up considerably [17]. The key observation is that the evolution operator can be rearranged to use different time steps for the nuclear and electronic degrees of freedom. We can roughly estimate the ratio between the time steps to be $N = \sqrt{\mu_{pd}/\mu_e}$, assuming that the energy pumped into the nuclear motion by the field is the same as for the electrons. The rearranged time evolution operator is

$$U(t+\delta,t) = U_{T_\xi}\left(\frac{\delta}{2}\right)\prod_{i=1}^{N}\left[U_V\left(\frac{\delta}{2N};t_i\right)U_{T_\rho}\left(\frac{\delta}{N}\right)\times U_{T_z}\left(\frac{\delta}{N}\right)U_V\left(\frac{\delta}{2N};t_i\right)\right]U_{T_\xi}\left(\frac{\delta}{2}\right). \tag{15}$$

The electronic coordinates thus become updated N times more often than the nuclear coordinates. The rough estimate above gives $N \approx 35$. Testing, however, shows that N should be closer to 10. With $N=10$, we estimate that Eq. (15) requires 20%–25% fewer operations than Eq. (14). In the limit of large N, the same estimate gives an operations reduction of close to 30%.

2. Bound states

For all of the calculations reported in our previous work, the initial state for the propagation was the ground state of the molecular ion, i.e., the ground $1s\sigma$ vibrational state with σ electronic symmetry. This state was calculated as a solution of the time-independent Schrödinger equation with the Hamiltonian $T+V_0$ as given by Eqs. (2) and (3) by propagation in imaginary time using the same finite difference grid and the evolution operator from Eq. (15). In this work we have also performed calculations for the first 9 excited vibrational states.

Although propagation in imaginary time for calculating excited state energies is commonly used, for instance, in many-body Monte Carlo calculations [44], excited state wave function calculations within the imaginary time propagation approach are not so common. One of the ways of calculating the excited states is imaginary time propagation complemented with subsequent orthogonalization with respect to the states that are already calculated. In [45] it was proposed to propagate and orthogonalize several states simultaneously. Here, we suggest a more general point of view on the imaginary time propagator as a useful spectral transformation and discuss the ways of using this transformation for calculating the lowest eigenvalues and eigenvectors of a discretized Hamiltonian. A more complete discussion is in preparation.

Suppose H is a discretized Hamiltonian, E_n are its eigenvalues, and $|n\rangle$ are the corresponding eigenvectors. We shall assume that $E_1 < E_2 < \ldots < E_n$. Consider the imaginary time propagator

$$U_\delta = e^{-H\delta}.$$

Obviously, $[U_\delta, H]=0$ and the eigenvectors of U_δ and H coincide. The eigenvalues of the operator U_δ are $\lambda_k = e^{-E_k\delta}$. The imaginary time propagator, therefore, maps the minimal eigenvalues of H onto the maximal eigenvalues of the operator U_δ. In principle, any method of maximal eigenvalue calculation can be used. From this point of view, the traditional propagation in imaginary time corresponds to the simplest power method [43] with an error estimation for the ground state wave function at the nth step of the algorithm $O((\lambda_2/\lambda_1)^n)$ or $O(e^{-(E_2-E_1)n\delta})$, where δ is the time step of the algorithm and n is the number of propagation steps. If several eigenvalues and eigenvectors are required, however, a more appropriate approach can be based on the Arnoldi algorithm [43]. Besides providing the ability to calculate several eigenpairs, it also provides a better convergence rate. For instance, if the two minimal eigenvalues of $\hat{H}$ are close to each other, i.e., $|\lambda_1 - \lambda_2| \ll |\lambda_2|$, the error for the ground state eigenvector can be estimated as $O(e^{-2n\sqrt{(\lambda_1-\lambda_2)/\lambda_2}}) \approx O(e^{-2n\sqrt{(E_2-E_1)t}})$, which is substantially better than for the propagation in imaginary time.

The estimates we have just discussed are based on the assumption that the evolution operator can be calculated exactly. In practical calculations, however, usually some approximate evolution operator must be used. In the present work we, of course, use Eq. (15).

We show the energies of the molecular bound states calculated in this work in Table I. For reference purposes we also provide results of precise multichannel calculations of the HD$^+$ bound state energies from [42]. The difference does not exceed 0.2%, which can be considered a very good agreement.

TABLE I. Bound state energies for the lowest ten HD$^+$ bound states used in this work compared to the results of Ref. [42].

v	Ref. [42]	This work	Relative difference
0	−0.59803	−0.59723	0.13%
1	−0.58932	−0.58864	0.11%
2	−0.58104	−0.58003	0.17%
3	−0.57319	−0.57252	0.12%
4	−0.56575	−0.56532	0.08%
5	−0.55871	−0.55823	0.09%
6	−0.55207	−0.55158	0.09%
7	−0.54582	−0.54534	0.09%
8	−0.53996	−0.53937	0.11%
9	−0.53447	−0.53396	0.10%

III. RESULTS

We have studied ionization and dissociation of several ($v=0\ldots9$) vibrational states of the HD$^+$ molecule in a short laser pulse. The laser pulse carrier wavelength was chosen to be $\lambda=790$ nm, and the pulse envelope has a Gaussian profile with 7.1 fs intensity FWHM width. The calculations were performed for the peak intensities of $I_0=0.5,0.8,1.0,2.0,4.0,7.0\times10^{14}$ W/cm^2. To keep the discussion simple, we consider an oriented initial state of the molecule, with the d ion up and the p ion down. However, as discussed in Ref. [17], after an appropriate averaging the results are also valid for unoriented, aligned molecules. First, we shall report our total dissociation and ionization probabilities for different initial vibrational states. The rest of the discussion will be devoted to CEP effects in dissociation of HD$^+$. For instance, how do the CEP effects vary with the laser pulse intensity and the initial vibrational state? Can we identify the conditions favorable for observing CEP effects? How can CEP effects in dissociation be observed for an incoherent sum of initial vibrational states?

A. Initial-state dependence

Both ionization and dissociation demonstrate strong dependence on the laser intensity and the initial state of the system. As shown in Fig. 2, it is clearly seen that when the peak intensity of the pulse increases, more tightly bound vibrational states start dissociating as expected. For instance, whereas for the moderately low peak intensity of 10^{13} W/cm^2 the lowest state with appreciable dissociation is $v=7$, at 5×10^{13} W/cm^2 states down to $v=4$ dissociate, and at 4×10^{14} W/cm^2 there is a considerable dissociation from all vibrational states. This trend can be easily explained from the adiabatic Floquet potentials at each intensity in terms of bond softening and above-threshold dissociation [3].

For the present wavelength of 790 nm, the bond-softening crossing in the adiabatic potentials occurs at an energy near the $v=9$ energy level; the above threshold dissociation crossing near $v=3$. As the intensity increases, the gap at each crossing grows, pushing the corresponding barriers lower uncovering deeper vibrational states. At intensities below roughly 10^{14} W/cm^2, bond softening dominates and the dissociation probability decreases monotonically with decreasing v. At higher intensities, though, this monotonic behavior is lost as above-threshold dissociation—which, again, is resonant close to $v=3$—grows. At 4×10^{14} W/cm^2, in particular, the dissociation probability for $v=3$ is noticeably larger than for neighboring states.

In Fig. 2, it is also clear that higher vibrational states ionize more readily. Ionization is significant, though, only for

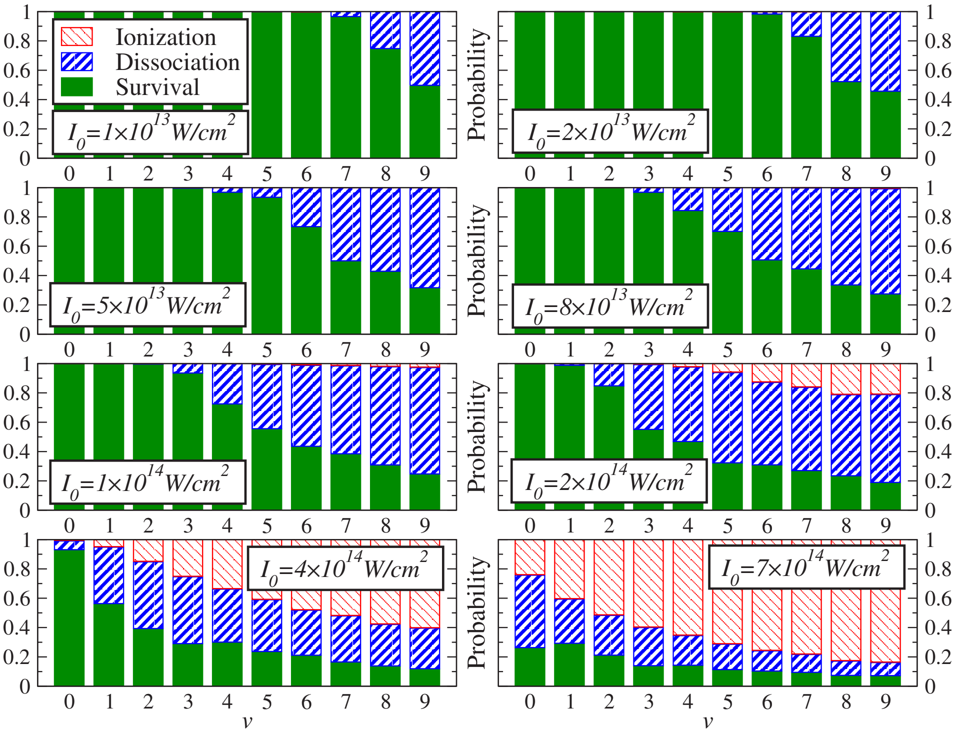

FIG. 2. (Color online) Initial vibrational state dependence of ionization and dissociation for several peak laser intensities.

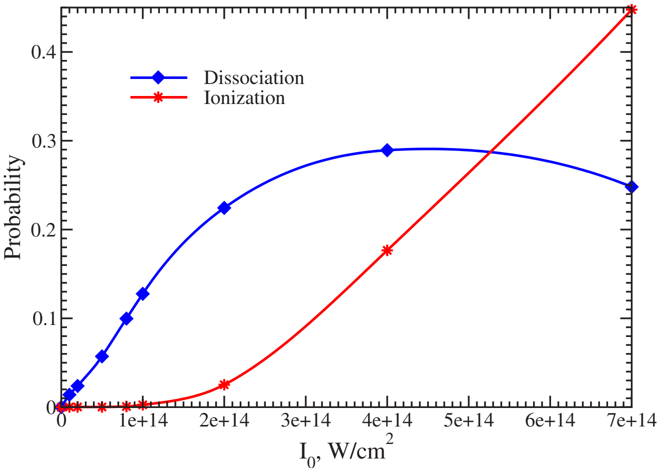

FIG. 3. (Color online) Intensity dependence of Franck-Condon-averaged dissociation and ionization probabilities.

intensities of 10^{14} W/cm^2 and higher, and all states ionize with appreciable probability by 7×10^{14} W/cm^2. Ionization of $v=9$ has only reached a little over 80% at this intensity, however, with the remaining probability split between dissociation and survival. These latter probabilities presumably decrease for longer laser pulses.

B. Intensity dependence of Franck-Condon-averaged total ionization and dissociation

Dissociation from a single vibrational state, however, is not a situation currently available experimentally, since such molecular targets are very difficult to prepare. Instead, the initial states of the molecular ions experimentally available depend on the ion source. In this paper we assume that the HD^+ ions are produced with some fast process, such as impact ionization of the neutral molecule. In this case the initial distribution can be well approximated with a Franck-Condon (FC) distribution. We also assume that the ion travel times differ enough to dephase the vibrational states. In this case, the experimentally observed results will be an incoherent sum of the results produced by individual initial states. For this reason we have averaged the dissociation and ionization probabilities from individual vibrational states over the Franck-Condon distribution. The FC-weighted total dissociation and ionization probabilities are shown in Fig. 3. Dissociation dominates over ionization for all intensities up to about 5×10^{14} W/cm^2. For intensities below 1×10^{14} W/cm^2, it is the only significant breakup channel.

Franck-Condon averaging, however, is not the only experimental complication. The distribution of the laser intensity over the focal volume makes an intensity average necessary when the target is larger than the focal spot. The exact connection between the experimental observable N (counts, counting rates, etc.) and the calculated probabilities $P(I)$ depend on the geometry of the experiment. For concreteness, we will assume an experimental geometry appropriate for the ion-beam experiments of Ben-Itzhak *et al.* [22]. That is, we assume a cylindrically symmetric Gaussian intensity profile for a laser beam that intersects a molecular ion beam at right angles. The ion beam is large compared to the focal spot size, but small compared to the Rayleigh length. We must thus average over a two-dimensional intensity distribution,

$$N \propto \int_0^{I_0} \frac{P(I)}{I} dI.$$

The proportionality constant in this equation is not important as the experiments are not absolute.

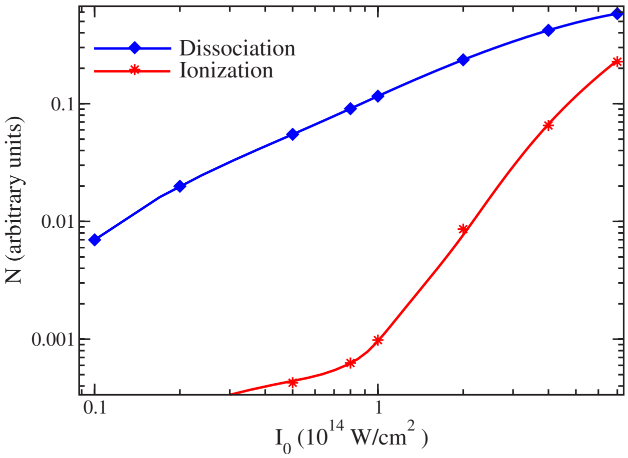

FIG. 4. (Color online) Intensity dependence of focal volume and Franck-Condon-averaged dissociation and ionization.

In Fig. 4 we show N for dissociation and ionization. Since the maximal field strength is achieved only in a small fraction of the focal volume, signals from the highest intensity region do not contribute nearly so much as lower intensities to N. Because of this, the dissociation channel strongly dominates over the ionization channel over the whole range of intensities after focal volume (or intensity) averaging. The growth of N for ionization is much faster, however: when increasing the peak intensity from 5×10^{13} W/cm^2 to 5×10^{14} W/cm^2, we predict two orders of magnitude growth in the ionization channel but only one order of magnitude for dissociation.

C. Carrier-envelope phase effects in channel probabilities

All the aforementioned results were averaged over the carrier-envelope phase and correspond to experiments where the CEP is not stabilized and changes randomly from one pulse to another. Now we will concentrate on discussing the CEP effects.

To describe a CEP effect we have to specify an observable that is affected by the CE phase. In atomic photoionization [15,16], for instance, CEP effects were observed in the angular distribution of the photoelectron. It has also been suggested that CEP effects can be observed in atomic excitation probability [21]. Our previous and present predictions are more like the former—we suggest measuring the angular distribution of the heavy fragments in photodissociation. Although there has been a measurement along these lines [19], that experiment used neutral D_2 as a target. This difference has two main consequences: (1) the initial distribution of D_2^+ vibrational state is coherent and (2) the rescattering of the

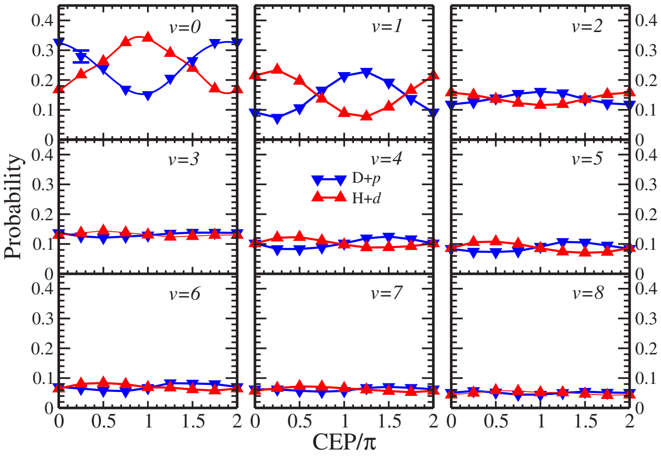

FIG. 5. (Color online) Dissociation from different initial vibrational states into the H+d and D+p as a function of the CEP for the peak intensity I_0=7×10^{14} W/cm^2. The numerical error is comparable with the size of the triangles.

ionized electron plays a critical role. Neither of these applies to the present case, however. Moreover, given the strong dependence of ionization on CEP [15,16] and the importance of rescattering on the experiment of Kling *et al.* [19], we can expect that the physical mechanisms leading to CEP effects are different in the two cases.

For our model with aligned and oriented nuclei that are not allowed to rotate the angular distribution corresponds to a charged particle leaving in the direction of positive or negative z. In our model—with only nuclear vibration—we also assume that the nuclei cannot switch places due to their Coulomb repulsion, thus a charged particle leaving along $z > 0$ is associated with H+d fragmentation and along $z<0$ to D+p. We have thus focused on comparing the probabilities H+d and D+p [17]. With this picture in mind, we expect that there will be a similar "up"-"down" asymmetry for H_2^+ and D_2^+ as well. In fact, we showed that H_2^+ does indeed behave similarly in [17], although the magnitude of the effect was smaller than for HD$^+$. Our present calculations confirm our earlier prediction that the probability of dissociation from the ground state varies significantly with the CEP for the intensities about 7×10^{14} W/cm^2 (see Fig. 5). For example, the maximal and minimal values of the dissociation probabilities in each of the channels can differ by as much as a factor of 2 for $v=0$ and three for $v=1$. Dissociation from other vibrational states up to $v=5$ also demonstrate a clear CEP dependence. Each vibrational state, however, demonstrates different CEP dependence. Since measurement of the dissociation from a single vibrational state is difficult to realize experimentally, a question naturally arises: can we observe a CEP effect in dissociation after Franck-Condon averaging?

In Fig. 6 we show the Franck-Condon-averaged dissociation probability as a function of CEP for several intensities. Even though there was strong CEP dependence in dissociation from individual vibrational states, FC averaging significantly weakens the effect. In particular, for peak intensities of 2×10^{14} W/cm^2 and below, our calculations show no CEP effect since the amplitude of the variation of the channel probabilities is comparable to our numerical error. After focal volume averaging (Fig. 7), the effect becomes comparable to the numerical error of our calculations for all intensities, thus, even if there remains a real effect beyond our numerics, measuring put quite stringent requirements on the counting statistics.

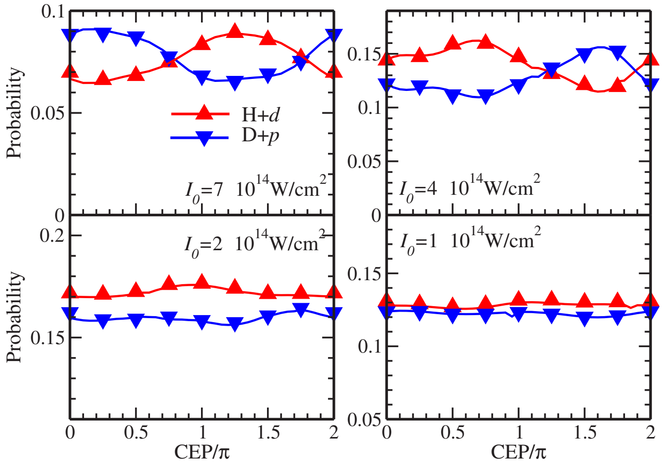

FIG. 6. (Color online) Franck-Condon-averaged channel dissociation probabilities as a function of CEP. Compared with Fig. 5, a weaker but clear effect is visible at higher peak intensities, but practically no effect can be expected below I_0=2×10^{14} W/cm^2. The numerical error is comparable with the size of the triangles.

D. KER of the dissociated fragments

Another observable that can be directly measured in experiment, besides the total channel probabilities, is the KER distribution of the fragments in each channel. Figure 8 shows the CEP-averaged KER distributions for a number of laser peak intensities. We note that from this point on, all results include Franck-Condon averaging. The KER distributions are shown for the both H+d and D+p channels. The observed difference in the KER is comparable to the numerical

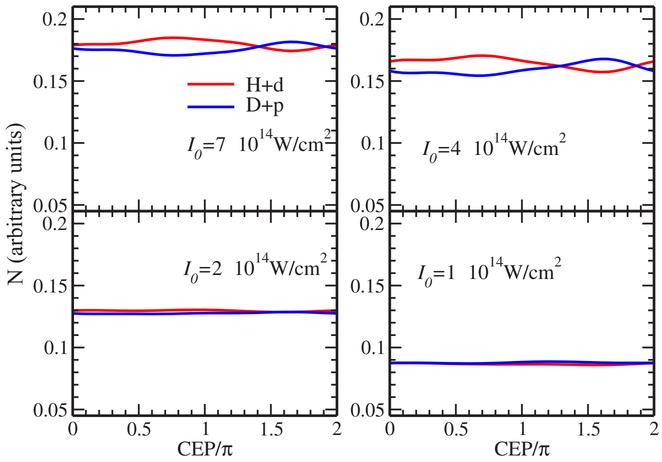

FIG. 7. (Color online) The CEP effect in the total channel dissociation probabilities, including Franck-Condon and focal volume averaging. The effect does not exceed the numerical error.

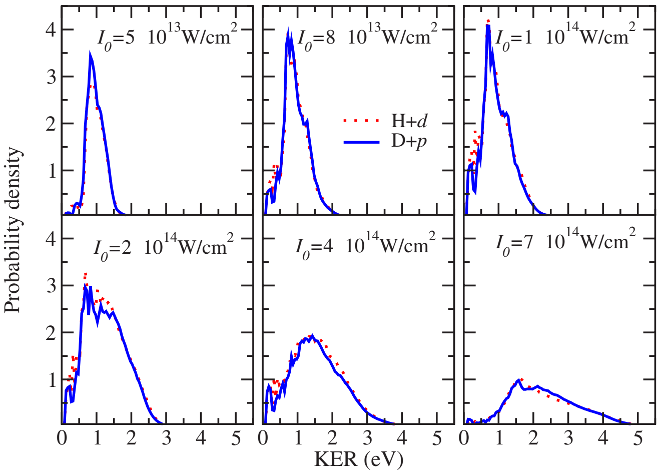

FIG. 8. (Color online) CEP-averaged kinetic energy release (KER) distributions of the dissociated fragments for different peak intensities, including Franck-Condon averaging.

error of our calculations showing that there is no appreciable inherent asymmetry for this system. Any such asymmetry we find can thus be ascribed to CEP effects. As the peak intensity grows, the KER distribution spreads toward higher energies. This point is especially clear for intensities above 2×10^{14} W/cm^2, where the tail of the distribution extends up to 5 eV at 7×10^{14} W/cm^2. For lower intensities the tail reaches out only to 1.5–2 eV. Moreover, these low-intensity KER distributions peak at around 0.8 eV where we expect bond-softening contributions to dominate at 790 nm. This behavior is consistent with experiment [22], as is the broadening of the distributions, first to low KER, then to high KER, with increasing intensity. In particular, from the discussion of Fig. 8 we expect above-threshold dissociation to start contributing significantly at around 4×10^{14} W/cm^2—precisely where the KER starts broadening to higher values.

The KER, however, can be a much more sensitive tool for investigating CEP effects than the total channel probabilities. The channel probabilities include contributions from fragments of very different kinetic energies. The KER is a dynamical quantity and can thus be expected to be more sensitive to delicate features of the dynamics. This expectation was confirmed by our earlier results [18], and here we present a more detailed study of the KER CEP sensitivity. We showed in Ref. [18], for instance, that the ratio between the maximum and minimum of the KER density function can be over 100 for the ground vibrational state, which would definitely allow a clear observation of the effect. Since this experiment is not likely to be done soon, though, we must include Franck-Condon averaging and the focal volume averaging, both of which tend to make the CEP contrast smaller. Here, we address the question how these complications affect the contrast in the KER distributions.

First, we consider FC averaging. The fragment KER for the D+*p* channel is shown in Fig. 9. The KER for the H+*d* channel looks very similar but with a translation in CEP by π, although the accuracy of our calculations does not make it possible for us to comment any possible effects of small mass asymmetry of the two channels. We show the KER distributions with a resolution of 0.1 eV, which is not difficult to achieve experimentally [23]. One interesting point about the KER CEP dependence is that unlike the channel probabilities which showed significant CEP dependence only for high intensities, we can observe some CE phase dependence in the KER even at the moderate intensity of $I_0=5\times10^{13}$ W/cm^2 (Fig. 9).

E. Carrier-envelope phase sensitivity of the KER

In order to specify conditions of the CEP observability more accurately, it is useful to introduce a measure of the effect. We quantify the sensitivity of a quantity $q(\phi)$ to the CE phase ϕ through $q_{\max}=\max_\phi q(\phi)$ and $q_{\min}=\min_\phi q(\phi)$, the maximum and minimum of q over the whole range of ϕ. One measure of the strength of CEP effects is thus

$$S_q=\frac{q_{\max}-q_{\min}}{q_{\max}}. \qquad (16)$$

This definition assumes q to have non-negative values and could have just easily been normalized by the average value instead of the maximum. Clearly, the larger the CEP effects in q, the larger S_q will be.

In Fig. 10 we show the strength of the CEP effect (16) for the KER of dissociated fragments with one slight modification. Because our calculations have finite accuracy, we have introduced a small correction to S_q for Fig. 10:

$$S_q=\frac{q_{\max}-q_{\min}}{q_{\max}+\delta_q}.$$

We take δ_q to be a measure of the smallest value of the probability density that we are confident in. The goal of this modification is to eliminate from the plot large values of S_q that are most likely the result of numerical error.

We see from Fig. 10 that even at the relatively low intensity $I_0=5\times10^{13}$ W/cm^2, we can expect substantial variation of the number of fragments in the energy ranges 1.1±0.1 eV and 1.4±0.1 eV. When the peak intensity grows even slightly to $I_0=8\times10^{13}$ W/cm^2, the CEP effect becomes very visible—over 60% variation—at fragment energies close to 1 eV and 1.5 eV. As the intensity increases, strong CEP effect extends to higher energies. At $I_0=2\times10^{14}$ W/cm^2, the effect strength drops below 50%. At this intensity, ionization starts playing an important role in the dynamics of the system (see Fig. 5), especially for the higher vibrational states that contributed to dissociation at lower intensities. With further peak intensity growth, we see a clear effect again as lower vibrational states start contributing to dissociation. Comparing with the CEP-averaged KER distributions in Fig. 8, we see that the strongest CEP effects come at higher KERs, above the peak in the CEP-averaged distributions.

Now we are ready to address the question of volume averaging. The gray lines in Fig. 10 show the focal averaged CEP effect strengths. Their behavior is much the same as for the single peak intensities discussed above. The complete

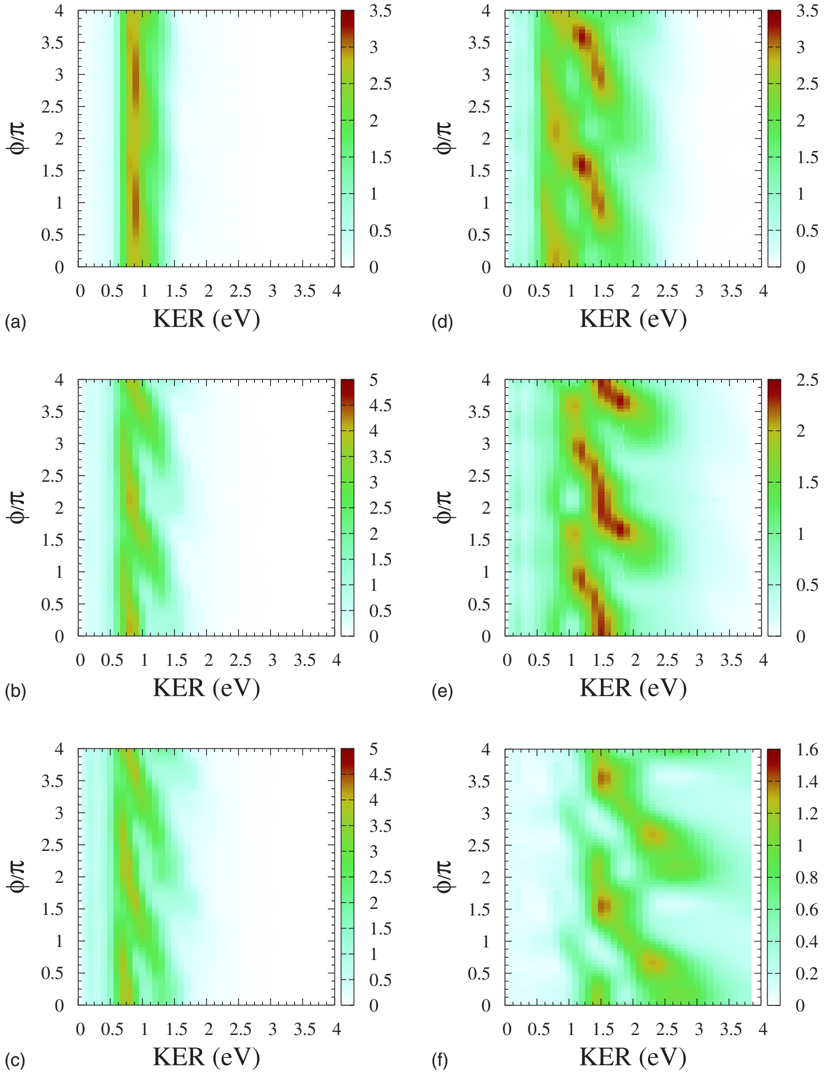

FIG. 9. (Color online) KER-CEP dependence of the D+p channel for different peak laser intensities: (a) $I_0 = 5\times10^{13}$ W/cm^2; (b) $I_0 = 8\times10^{13}$ W/cm^2; (c) $I_0 = 1\times10^{14}$ W/cm^2; (d) $I_0 = 2\times10^{14}$ W/cm^2; (e) $I_0 = 4\times10^{14}$ W/cm^2; (f) $I_0 = 7\times10^{14}$ W/cm^2. Two periods of the CEP are shown. Franck-Condon averaging is included.

volume-averaged KER distributions of the fragments in the D+p channel are shown in Fig. 11. We see that the strong contribution of low intensities changes the picture dramatically. Even though the KER distribution varies with the CEP within 20 to 30 % (Fig. 10), this variation is only about half that expected for a single intensity.

If an experiment is sensitive enough to measure the tail of the KER distribution accurately, however, a clear effect can be seen again. Lower intensities contribute little to energies above 2 eV, and this is exactly the range where Fig. 10 suggests the strongest CEP effects lie. To make the CEP effects in the tail of the KER distribution clear it is useful to renormalize the signal by its CEP-averaged value. The results are shown in Fig. 12. We have hidden regions where our numerical error exceeds the predicted signal. After the renormalization, the CEP effect is again visible, and the effect can be clearly seen for all the sampled peak intensities. We note that the diagonal stripes in Fig. 12 appear only after Franck-Condon averaging. Individual vibrational states do have structure, but not stripes. These stripes are thus not directly the result of interference since Franck-Condon averaging is incoherent.

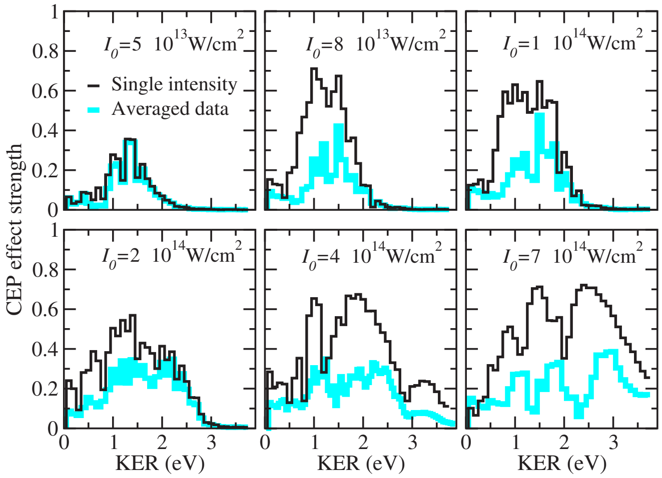

FIG. 10. (Color online) KER dependence of the CEP effect strength (16) for different peak laser intensities. The error parameter is set to $\delta = 0.3$, a conservatively estimated accuracy of our KER distribution calculations. Thin black lines denote a single peak intensity; thick cyan lines denote focal volume averaged results. Franck-Condon averaging is included.

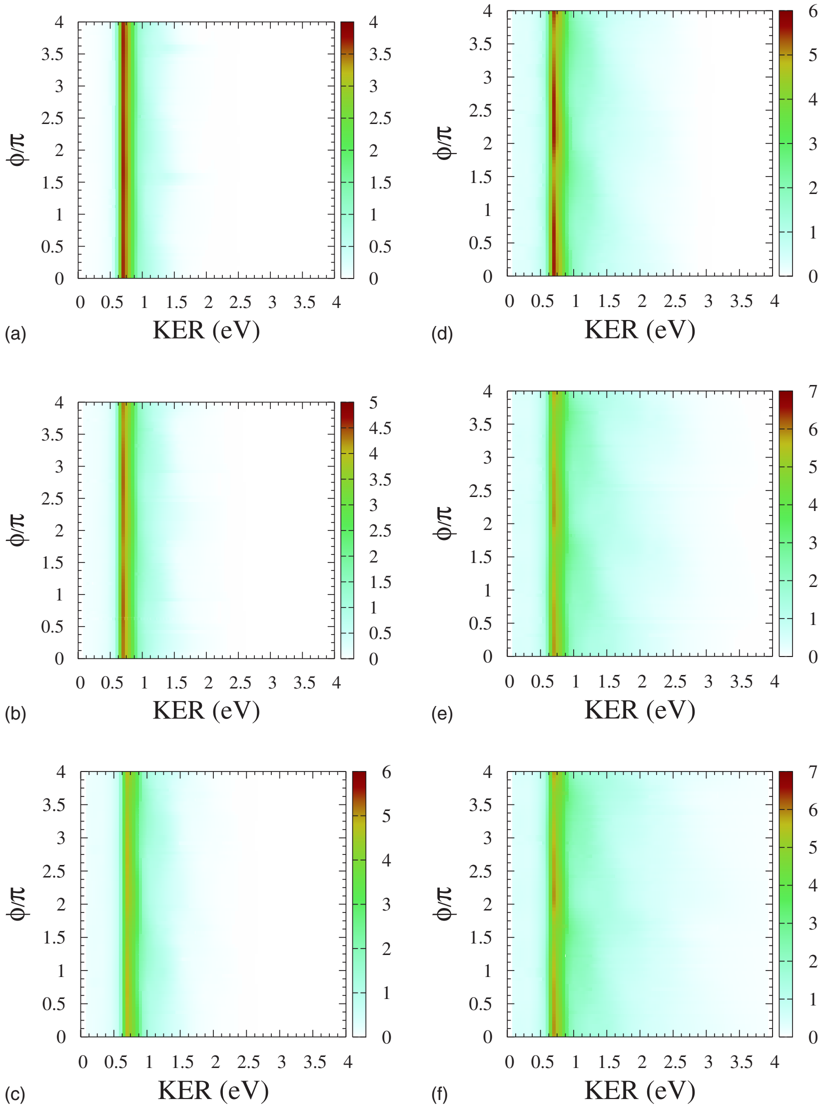

FIG. 11. (Color online) Focal volume averaged KER-CEP dependence of the D+p channel for different peak laser intensities: (a) $I_0=5\times10^{13}$ W/cm^2; (b) $I_0=8\times10^{13}$ W/cm^2; (c) $I_0=1\times10^{14}$ W/cm^2; (d) $I_0=2\times10^{14}$ W/cm^2; (e) $I_0=4\times10^{14}$ W/cm^2; (f) $I_0=7\times10^{14}$ W/cm^2. Two periods of the CEP are shown. Franck-Condon averaging is included.

IV. SUMMARY AND DISCUSSION

Now we can answer the question: where should we look if we want to observe CEP effects in HD$^+$ dissociation and how big is the effect? We shall also mention gross features of the system that should accompany observable CEP effects.

If we want to see an effect in the angular distribution of the outgoing fragments without measuring their KER, we should use pulses with peak intensities above $I_0=2\times10^{14}$ W/cm^2. A threefold variation of the signal can be expected for dissociation from $v=0$ or $v=1$. Franck-Condon averaging, though, reduces the variation to less than roughly 20%, and the effect does not survive focal volume averaging. To have a chance of seeing an effect, then, focal volume averaging must be reduced or eliminated experimentally using either an effective one-dimensional (1D) geometry [24] or intensity-differential measurements [25]. If the intensity is in the appropriate range, the total dissociation probability is expected to be comparable with the probability of ionization, and should not exceed it by more than 60%.

In any case, measuring the KER distribution makes observing CEP effects much more likely, since the KER distribution is much more sensitive to the CEP than the angular distributions alone. If the experimental conditions can also guarantee contribution of only a small range of intensities to the signal, the effect can be seen for much lower intensities. For instance, we can expect a clear effect to be seen even below $I_0=10^{14}$ W/cm^2, when no substantial ionization is predicted. For all intensities above $I_0=10^{14}$ W/cm^2, we expect considerable ionization, which is expected to accompany strong CEP effects in the KER distribution. These effects are especially clear on the high-energy tail of the KER distribution, at energies above 1 eV. The regions of the best contrast are intensity dependent, and the contrast itself is not a monotonic function of intensity. For lower intensities from 5×10^{13} to 10^{14} W/cm^2, the best contrast is expected for the KER close to 1 eV and 1.5 eV. For higher intensities the regions of the best contrast vary. For instance, we expect the CEP effect to be well pronounced in the KER range from 2 to 2.5 eV.

If the experimental geometry and efficiency, however, do not admit sharp and reliable intensity separation, the CEP effect in the KER can still be seen in focus volume averaged results. In this case the best contrast is expected at the very

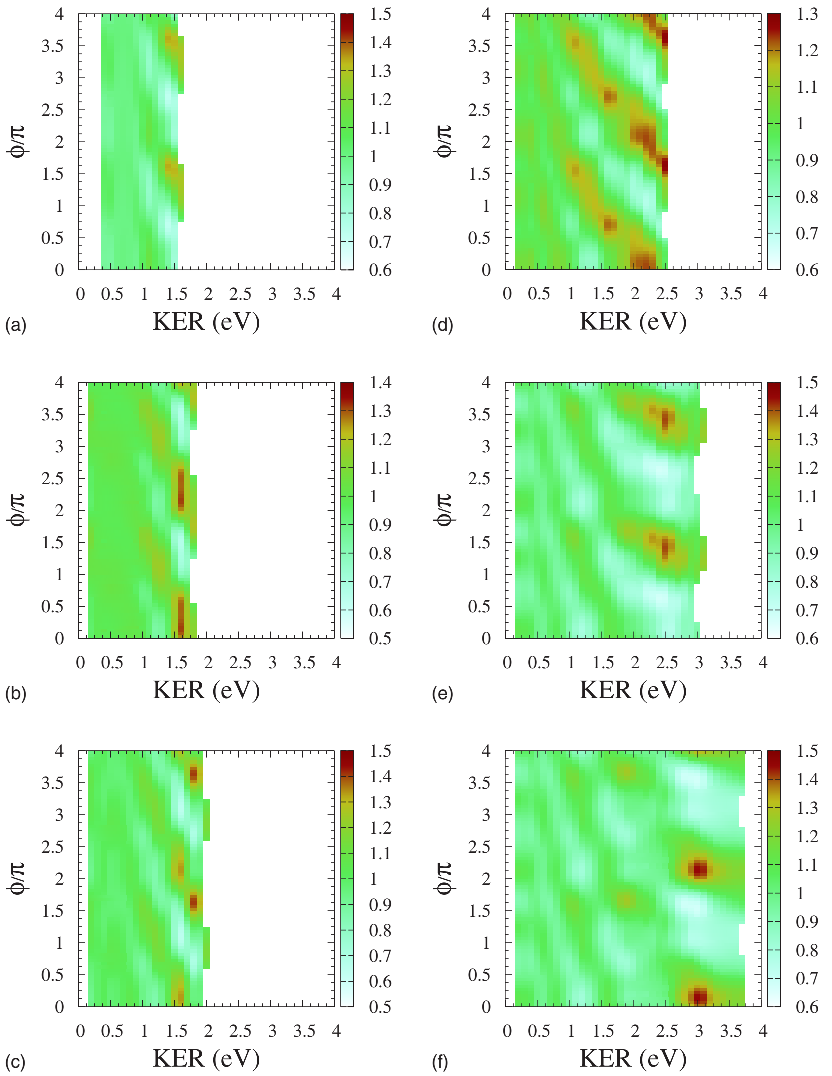

FIG. 12. (Color online) Focal volume averaged KER-CEP dependence for D+p channel normalized within each KER bin (see text). Each panel shows a different peak laser intensity: (a) $I_0=5\times10^{13}$ W/cm^2; (b) $I_0=8\times10^{13}$ W/cm^2; (c) $I_0=1\times10^{14}$ W/cm^2; (d) $I_0=2\times10^{14}$ W/cm^2; (e) $I_0=4\times10^{14}$ W/cm^2; (f) $I_0=7\times10^{14}$ W/cm^2. Two periods of the CEP are shown. Regions where the estimated numerical error exceeds the predicted signal are hidden. Franck-Condon averaging is included.

end of the KER distribution tail. As the KER distribution extends toward higher fragment energies when the intensity increases, it automatically guarantees that the higher KER tail of the distribution is formed by a small range of intensities only. This helps to make the CEP effect well visible even after volume averaging.

ACKNOWLEDGMENTS

This work was supported by the Chemical Sciences, Geosciences, and Biosciences Division, Office of Basic Energy Sciences, Office of Science, U.S. Department of Energy. The authors wish to thank I. Ben-Ithzak, P. Q. Wang, A. M. Sayler, and K. D. Carnes for many fruitful discussions.

---

[1] A. Zavriyev, P. H. Bucksbaum, H. G. Muller, and D. W. Schumacher, Phys. Rev. A **42**, 5500 (1990).

[2] A. Giusti-Suzor, X. He, O. Atabek, and F. H. Mies, Phys. Rev. Lett. **64**, 515 (1990).

[3] A. Giusti-Suzor and F. H. Mies, Phys. Rev. Lett. **68**, 3869 (1992).

[4] E. E. Aubanel, J. M. Gauthier, and A. D. Bandrauk, Phys. Rev. A **48**, 2145 (1993).

[5] G. Yao and Shih-I Chu, Phys. Rev. A **48**, 485 (1993).

[6] T. Zuo, S. Chelkowski, and A. D. Bandrauk, Phys. Rev. A **48**, 3837 (1993).

[7] A. Datta, S. Saha, and S. S. Bhattacharyya, J. Phys. B **30**, 5737 (1997).

[8] S. Chelkowski and A. D. Bandrauk, J. Phys. B **28**, L723 (1995).

[9] S. Chelkowski, T. Zuo, O. Atabek, and A. D. Bandrauk, Phys. Rev. A **52**, 2977 (1995).

[10] T. Seideman, M. Yu. Ivanov, and P. B. Corkum, Phys. Rev. Lett. **75**, 2819 (1995).

[11] L. B. Madsen and M. Plummer, J. Phys. B **31**, 87 (1998).

[12] E. Charron, A. Giusti-Suzor, and F. H. Mies, J. Chem. Phys. **103**, 7359 (1995).

[13] A. Giusti-Suzor, F. H. Mies, L. F. DiMauro, E. Charron, and B. Yang, J. Phys. B **28**, 309 (1995).

[14] J. H. Posthumus, Rep. Prog. Phys. **67**, 623 (2004).

[15] G. G. Paulus *et al.*, Nature (London) **414**, 182 (2001).

[16] A. Baltuska, Th. Udem, M. Uiberacker, M. Hentschel, E. Goulielmakis, Ch. Gohle, R. Holzwarth, V. S. Yakovlev, A. Scrinzi, T. W. Hänsch, and F. Krausz, Nature (London) **421**, 611 (2003).

[17] V. Roudnev, B. D. Esry, and I. Ben-Itzhak, Phys. Rev. Lett. **93**, 163601 (2004).

[18] V. Roudnev and B. D. Esry, Phys. Rev. A **71**, 013411 (2005).

[19] M. F. Kling, Ch. Siedschlag, A. J. Verhoef, J. I. Khan, M. Schultze, Th. Uphues, Y. Ni, M. Uiberacker, M. Drescher, F. Krausz, and M. J. J. Vrakking, Science **312**, 246 (2006).

[20] I. Ben-Itzhak, P. Q. Wang, J. F. Xia, A. M. Sayler, M. A. Smith, K. D. Carnes, and B. D. Esry, Phys. Rev. Lett. **95**, 073002 (2005).

[21] T. Nakajima and S. Watanabe, Phys. Rev. Lett. **96**, 213001 (2006).

[22] P. Q. Wang, A. M. Sayler, K. D. Carnes, J. F. Xia, M. A. Smith, B. D. Esry, and I. Ben-Itzhak, Phys. Rev. A **74**, 043411 (2006).

[23] I. Ben-Itzhak (private communication).

[24] D. Pavičić, A. Kiess, T. W. Hänsch, and H. Figger, Phys. Rev. Lett. **94**, 163002 (2005).

[25] P. Wang, A. M. Sayler, K. D. Carnes, B. D. Esry, and I. Ben-Itzhak, Opt. Lett. **30**, 664 (2005).

[26] S. Chelkowski and A. D. Bandrauk, Phys. Rev. A **65**, 061802(R) (2002).

[27] H. Yu and A. Bandrauk, J. Chem. Phys. **102**, 1257 (1995).

[28] L. Y. Peng *et al.*, J. Phys. B **36**, L295 (2003).

[29] K. C. Kulander, F. H. Mies, and K. J. Schafer, Phys. Rev. A **53**, 2562 (1996).

[30] A. D. Bandrauk, S. Chelkowski, and I. Kawata, Phys. Rev. A **67**, 013407 (2003).

[31] B. Feuerstein and U. Thumm, Phys. Rev. A **67**, 043405 (2003); **67**, 063408 (2003).

[32] D. Dundas *et al.*, Eur. Phys. J. D **26**, 51 (2003).

[33] I. Kawata, H. Kono, and Y. Fujimura, J. Chem. Phys. **110**, 11152 (1999).

[34] S. Chelkowski, A. Conjusteau, T. Zuo, and A. D. Bandrauk, Phys. Rev. A **54**, 3235 (1996).

[35] E. A. Soloviev and S. I. Vinitsky, J. Phys. B **18**, L557 (1985).

[36] E. Y. Sidky and B. D. Esry, Phys. Rev. Lett. **85**, 5086 (2000).

[37] Z. X. Zhao, B. D. Esry, and C. D. Lin, Phys. Rev. A **65**, 023402 (2002).

[38] G. L. Ver Steeg, K. Bartschat, and I. Bray, J. Phys. B **36**, 3325 (2003).

[39] We convert between intensity I in $\mathrm{W/cm^2}$ and atomic units for the electric field using $E_0=\sqrt{I/3.5095\times 10^{16}\ \mathrm{W/cm^2}}$.

[40] M. W. J. Bromley and B. D. Esry, Phys. Rev. A **69**, 053620 (2004).

[41] W. H. Press, S. A. Teukolsky, W. T. Vetterling, and B. P. Flannery, *Numerical Recipes*, 2nd ed. (Cambridge University Press, Cambridge, 1992), pp. 640–642.

[42] B. D. Esry and H. R. Sadeghpour, Phys. Rev. A **60**, 3604 (1999).

[43] Y. Saad, *Numerical Methods for Large Eigenvalue Problems* (Halstead Press, Ultima, Australia, 1992).

[44] P. Huang, A. Viel, and K. B. Whaley, in *Recent Advances in Quantum Monte Carlo Methods, Part II*, edited by W. A. Lester, Jr., S. M. Rothstein, and S. Tanaka (World Scientific, Singapore, 2002), p. 111.

[45] P. Žďánska, D. Nachtigallováa, P. Nachtigall, and P. Jungwirth, J. Chem. Phys. **115**, 5974 (2001).